Electrochimica Acta 286 (2018) 158–162

Contents lists available at ScienceDirect

Electrochimica Acta

journal homepage: www.elsevier.com/locate/electacta

Lithium dissolution/deposition behavior with Li_3PS_4-LiI electrolyte for all-solid-state batteries operating at high temperatures

Motoshi Suyama, Atsutaka Kato, Atsushi Sakuda, Akitoshi Hayashi*, Masahiro Tatsumisago**

Department of Applied Chemistry, Graduate School of Engineering, Osaka Prefecture University, 1-1 Gakuen-cho, Naka-ku, Sakai, Osaka 599-8531, Japan

ARTICLE INFO

Article history:
Received 30 May 2018
Received in revised form
24 July 2018
Accepted 30 July 2018
Available online 1 August 2018

Keywords:
All-solid-state battery
Lithium battery
Lithium metal electrode
Sulfide electrolyte

ABSTRACT

The use of Li metal anode is important for developing all-solid-state Li rechargeable batteries with high energy densities. In this study, all-solid-state Li symmetric cells using sulfide electrolytes in the Li_3PS_4-LiI system were fabricated to investigate the Li dissolution/deposition cycling performance. A cell using $54Li_3PS_4 \cdot 46LiI$ (mol%) glass electrolyte was cycled at a current density of 1.25 mA cm^{-2} for 3400 h at 100 °C without short-circuiting, and the highest areal capacity of 7.5 mAh cm^{-2} was achieved. Structural analyses of the interface between Li and solid electrolytes revealed that the reduction of electrolyte by the Li metal was suppressed by adding LiI to Li_3PS_4, and good interfacial contact was maintained even after prolonged cycling. The addition of LiI to Li_3PS_4 glass improved the tolerance to reduction with Li metal, and enhanced the Li dissolution/deposition cycling performance.

1. Introduction

Li metal is a promising negative electrode material for high-energy-density batteries because it has high theoretical capacity (3860 $mAhg^{-1}$) and the lowest electrochemical potential (−3.04 V vs. SHE) [1]. However, Li metal rechargeable batteries have not been commercialized, because the growth of Li dendrites through the separator causes short-circuiting and raises safety concerns. To resolve these issues, the use of solid electrolytes has been extensively investigated. Reported solid electrolytes for all-solid-state cells with Li metal anodes include $Li_7La_3Zr_2O_{12}$ (LLZ) and lithium phosphorus oxynitride glass (LIPON) [2,3]. Li_2S-P_2S_5 glass electrolytes show high ionic conductivity above 10^{-4} S cm^{-1} and good formability to densify simply by cold pressing [4,5]. Densifying Li_2S-P_2S_5 glass electrolytes may reduce voids and grain-boundaries that lead to the growth of Li dendrite. We have reported higher Li dissolution/deposition performance for Li/Li_3PS_4 glass/Li cell when operated at 100 °C than at 25 °C [6]. The performance was further improved by inserting an Au buffer layer at the Li/Li_3PS_4 interface [6,7].

However, theoretical calculations suggested that upon contact with Li metal, Li_3PS_4 glass electrolytes decomposed to Li_2S and Li_3P, which are electrically insulating and thus passivate further decomposition of the electrolyte [8]. In fact, X-ray photoelectron spectroscopy (XPS) revealed that the decomposed layer consisting of Li_2S and Li_3P was formed only in the vicinity of the Li/Li_3PS_4 interface [9]. In cells using liquid electrolytes, the decomposed layer—called the solid electrolyte interphase (SEI) —plays an important role in Li dissolution and deposition [10–12]. Therefore, the interface layer should also affect Li dissolution/deposition in the all-solid-state cell.

Crystalline lithium halides are promising materials for stabilization of the Li/electrolyte interface, because they are thermodynamically stable against Li metal [8]. While it is difficult to use them as single electrolytes due to their low ionic conductivities, adding them to glass electrolytes can enhance the ionic conductivity [13–16]. We thus focus on the addition of lithium halides to Li_2S-P_2S_5 electrolyte as a third component. The addition of LiI to Li_2S-P_2S_5 glasses increases their ionic conductivities [14,17]. In addition, $Li_7P_2S_8I$ crystal (at the molar ratio of Li_3PS_4:LiI = 2:1) shows high electrochemical stability [18]. Therefore, the addition of LiI to Li_3PS_4 glass is expected to improve both the ionic conductivity and the electrochemical stability to Li metal. However, the effects of added LiI on the structure at the interface with Li metal have not been examined in detail.

In this study, the Li dissolution/deposition cycling performance

* Corresponding author.
** Corresponding author.
E-mail addresses: hayashi@chem.osakafu-u.ac.jp (A. Hayashi), tatsu@chem.osakafu-u.ac.jp (M. Tatsumisago).

https://doi.org/10.1016/j.electacta.2018.07.227
0013-4686/

of cells using Li_3PS_4-LiI electrolytes was investigated, and structural analysis of the Li/Li_3PS_4-LiI interface was conducted after Li dissolution/deposition. A Li symmetric cell using Li_3PS_4-LiI electrolytes was fabricated. Galvanostatic cycling tests for the cells were performed at 100 °C, because previous studies found that the Li dissolution/deposition performance was improved at 100 °C compared to 25 °C [6,19]. After the galvanostatic cycling tests, the structure and morphology of the Li/Li_3PS_4-LiI interface were analyzed by X-ray diffraction (XRD) and scanning electron microscopy (SEM).

2. Experimental

Samples of (100-*x*)Li_3PS_4-*x*LiI (mol%) electrolytes were prepared by mechanochemical processing. Reagent-grade Li_2S (99.9%; Mitsuwa Chemical Corp., Ltd.), P_2S_5 (99%; Aldrich Chemical Corp. Inc.), and LiI (99.999%; Aldrich Chemical Corp. Inc.) as starting materials were mixed in an agate mortar, and placed in a 45-mL ZrO_2 pot with 500 ZrO_2 balls 4 mm in diameter. The pot was set in a planetary ball mill (Pulverisette 7; Frich GmbH), and mechanochemical treatment was performed at 510 rpm for 10 h. The obtained powder was uniaxially pressed at 360 MPa into a pellet with a diameter of 10 mm. Li symmetric cells were assembled by attaching Li foils and stainless steel foils (current collector) to both sides of the electrolyte pellet. The cell was sealed in a laminate pouch under vacuum. Cold isostatic pressing (CIP) was conducted at 80 MPa to improve the contact between Li metal and the electrolyte layers.

The resistances of the cells of Li/(100-*x*)Li_3PS_4·*x*LiI/Li were characterized by the AC impedance method using an impedance analyzer (SI-1260; Solartron) at 25 °C and 100 °C. Galvanostatic cycling tests were carried out at 100 °C under a confining pressure of about 0.8 MPa using charge-discharge measuring devices (BTS-2004, Nagano Corp.). XRD measurements (SmartLab; Rigaku Corp.) were performed with Cu-K_α radiation. Raman spectroscopy was done using a spectrometer (LabRAM HR-800; HORIBA Ltd.) equipped with a green laser (532 nm). The morphologies of the Li/electrolyte interface were observed by SEM (SU8220; Hitachi Ltd.)

3. Results and discussion

Fig. 1a shows the XRD patterns of (100-*x*)Li_3PS_4·*x*LiI samples prepared by mechanochemical processing. Halo patterns were observed for samples with compositions of $x = 0$ and 46. Raman spectra of the prepared glasses, shown in Fig. 1b, indicated that the glasses were mainly composed of PS^{4-} ions, and there was no spectral change by the addition of LiI to Li_3PS_4. We confirmed that the crystallization temperature gradually decreased with increasing LiI content [17]. These results suggest that the LiI component was incorporated into the Li_3PS_4 glass matrix. The diffraction peaks assigned to LiI crystal were retained at 67 mol% LiI, indicating that this electrolyte was a composite of Li_2S-P_2S_5-LiI glass and LiI crystal.

The ionic conductivities of (100-*x*)Li_3PS_4·*x*LiI samples at 25 °C and 100 °C were estimated from the Nyquist plots of Li / (100-*x*) Li_3PS_4·*x*LiI / Li cells, as shown in Fig. 2. The ionic conductivity increased with increasing LiI content from 0 to 46 mol%, and the 54Li_3PS_4·46LiI glass showed the highest ionic conductivity of 2.1×10^{-2} S cm^{-1} at 100 °C. This value is comparable to that of Li_2S-P_2S_5-LiI glasses prepared by the melt-quench method [14]. However, the ionic conductivity decreased when the sample contained more than 46 mol% LiI, because at this point some of the LiI crystal

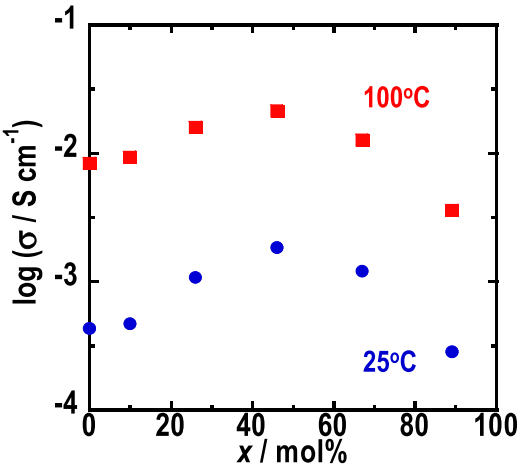

Fig. 2. Ionic conductivities of (100-*x*)Li_3PS_4·*x*LiI samples at 25 °C (blue circles) and 100 °C (red squares). (For interpretation of the references to colour in this figure legend, the reader is referred to the Web version of this article.)

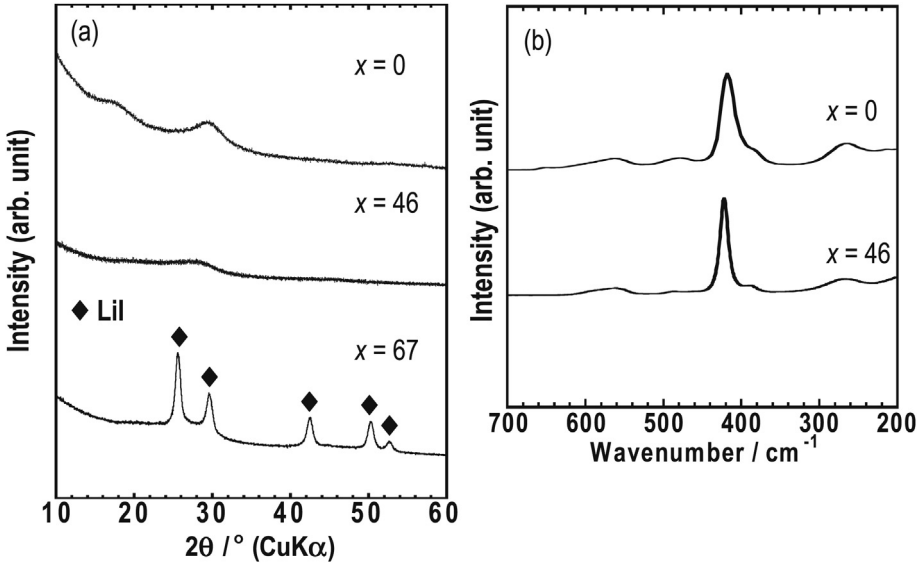

Fig. 1. (a) XRD patterns and (b) Raman spectra of (100-*x*)Li_3PS_4·*x*LiI samples.

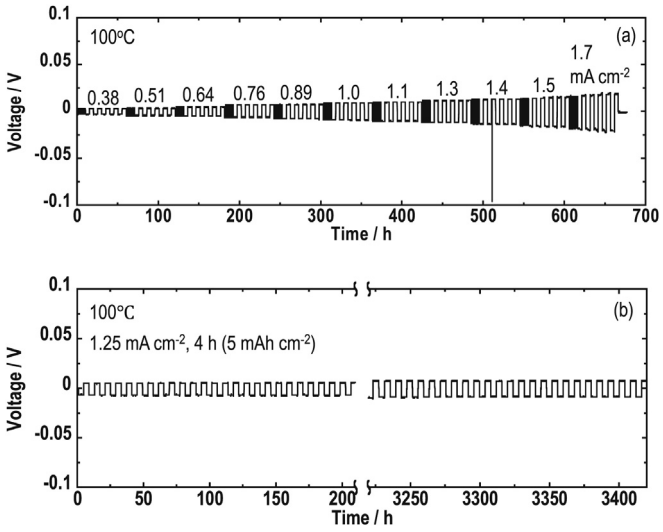

Fig. 3. (a) Galvanostatic cycling tests of Li/54Li_3PS_4·46LiI/Li cells at 100 °C. The applied current densities are shown in the figure. (b) Long-term galvanostatic cycling tests of Li/54Li_3PS_4·46LiI/Li at 100 °C. The applied current density was 1.25 mA cm^{-2}, and the areal capacity for a half cycle was 5 mAh cm^{-2}.

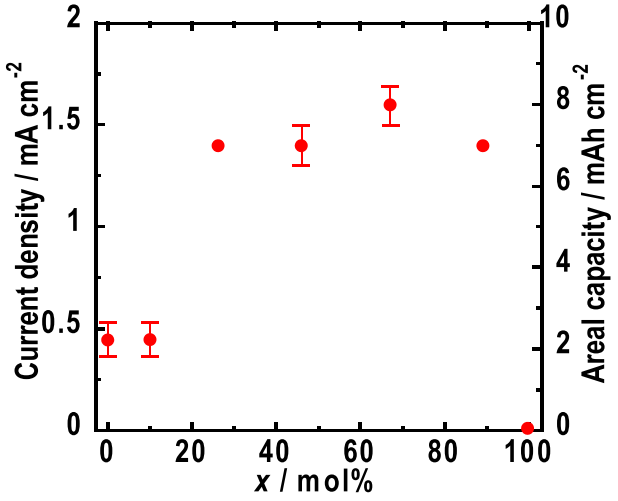

Fig. 4. Maximum current densities and areal capacities at which Li/(100-*x*)Li_3PS_4·*x*LiI/Li cells were cycled without short-circuiting. Galvanostatic cycling tests were conducted under the conditions shown in Fig. 3a.

with low conductivity remained [20].

To evaluate the Li dissolution/deposition performance of Li symmetric cells, galvanostatic cycling tests were conducted at 100 °C by applying a constant current for 1 or 5 h per half of the cycle. The current density was increased in a stepwise manner from 0.38 to 1.7 mA cm^{-2} after every 10 cycles (1 h for 5 cycles and 5 h for 5 cycles). The Li dissolution/deposition performance was defined as the maximum current density at which the cell was cycled without short-circuiting. As shown in Fig. 3a, the cell using 54Li_3PS_4·46LiI glass electrolyte was cycled at a high current density of 1.5 mA cm^{-2} for 5 h (7.5 mAh cm^{-2}) without short-circuiting. During that period, the thickness of Li metal changed by 37 μm during dissolution and deposition in half a cycle. A sudden drop of voltage was observed at a higher current density of 1.7 mA cm^{-2}, indicating that short-circuiting occurred due to inhomogeneous current distribution. In contrast, we have previously conducted the same experiment at 100 °C for a Li symmetric cell using Li_3PS_4 glass. The voltage fluctuated greatly even when the current density was as low as 0.64 mA cm^{-2}. The Li dissolution/deposition performance of the cell was improved by inserting Au thin films at the Li/Li_3PS_4 interface, since the cell was successfully cycled at 1.3 mA cm^{-2} for 5 h (6.5 mAh cm^{-2}) without short-circuiting [6]. In the current study, the cell using 54Li_3PS_4·46LiI glass electrolyte showed higher performance than that using Li_3PS_4 glass.

Long-term galvanostatic cycling tests were also performed. A constant current density of 1.25 mA cm^{-2} was passed for 4 h per half a cycle. As shown in Fig. 3b, the cell using 54Li_3PS_4·46LiI glass electrolyte did not short-circuit even after cycling for more than 3400 h (425 cycles). In addition, the voltage profile was stable, and no gradual increase in voltage was observed during cycling. This result indicates that the 54Li_3PS_4·46LiI glass shows good electrochemical stability against Li metal. Previously, long-term galvanostatic cycling tests were performed for cells using garnet-type electrolytes. Although those cells showed good cycling stability, their areal capacities were at most 0.5 mAh cm^{-2} [21–23]. In comparison, here we achieved stable Li dissolution/deposition at higher current density and areal capacity.

The Li dissolution/deposition performance as a function of LiI content was evaluated. Galvanostatic cycling tests were conducted under the condition shown in Fig. 3a. Fig. 4 shows the maximum current densities and areal capacities at which cells using (100-*x*) Li_3PS_4·*x*LiI electrolytes were cycled without short-circuiting. The performance was improved by adding LiI to Li_3PS_4 glass. The interfacial resistances between Li metal and Li_3PS_4-LiI glass in as-

Cell construction	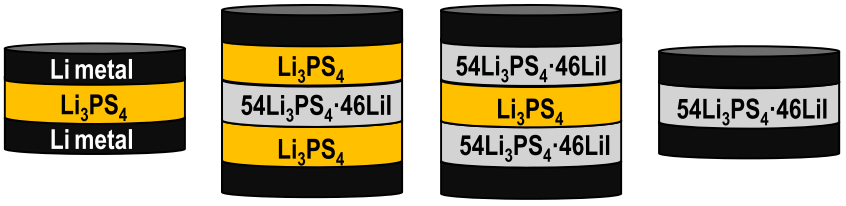			
	Li metal / Li_3PS_4 / Li metal	Li_3PS_4 / 54Li_3PS_4·46LiI / Li_3PS_4	54Li_3PS_4·46LiI / Li_3PS_4 / 54Li_3PS_4·46LiI	54Li_3PS_4·46LiI
Cell resistance / Ω	16	28	29	9
Maximum current density / mA cm^{-2}	0.38 - 0.51	0.51	1.3	1.3 – 1.5

Fig. 5. Resistances and maximum current densities of cells using Li_3PS_4 and 54Li_3PS_4·46LiI glass electrolytes.

prepared cells were about 1 Ω cm^2 regardless of the addition of LiI. Therefore, the contribution of the initial interfacial resistance to the electrochemical cycling performance seems small. When the LiI content was in the range of 67–89 mol%, the cell performance was similar to that of the cell using $54Li_3PS_4 \cdot 46LiI$ glass, although the LiI crystal partially remained and the ionic conductivity decreased at these compositions. However, the cell using LiI crystal showed lower performance than that using Li_3PS_4 glass. One possible reason is that LiI crystal has a low ionic conductivity of 10^{-6} S cm^{-1} even at 100 °C. This result indicates that the remaining LiI crystal does not contribute to the Li dissolution/deposition performance, while the glass matrix containing LiI is more important.

To investigate the reason why the Li dissolution/deposition performance was improved by addition of LiI to Li_3PS_4 glass, a cell with a triple-layer electrolyte pellet was fabricated using the Li_3PS_4 and $54Li_3PS_4 \cdot 46LiI$ glass electrolytes. The same experiment as shown in Fig. 4 was performed for these cells, and the results are summarized in Fig. 5. Both cells with triple-layer electrolyte pellets had the same resistance of about 30 Ω at 100 °C. However, the cell with $Li/54Li_3PS_4 \cdot 46LiI$ interface (the third one in Fig. 5) showed higher tolerance for short-circuiting than that with the Li/Li_3PS_4 interface (the second one), because the former had a higher maximum current density. Therefore, the solid electrolytes at the interface with Li metal were considerably important for preventing short-circuiting.

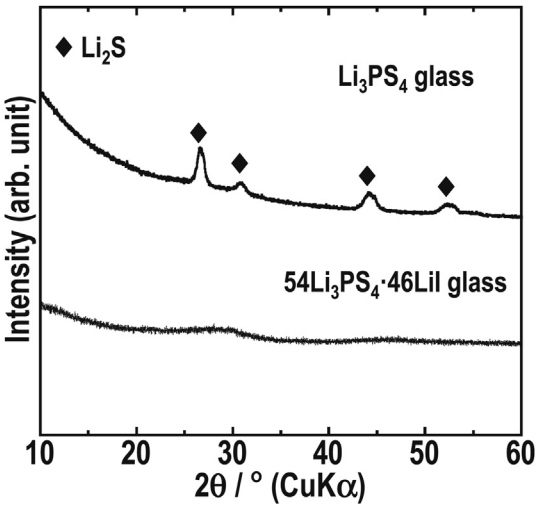

Fig. 6. XRD patterns of the surfaces of Li_3PS_4 and $54Li_3PS_4 \cdot 46LiI$ glass electrolytes after galvanostatic cycling tests at 100 °C.

After galvanostatic cycling tests at 100 °C, the structure and morphology of the interface between Li metal and solid electrolyte were evaluated. Fig. 6 shows XRD patterns of the surfaces of Li_3PS_4 and $54Li_3PS_4 \cdot 46LiI$ glass electrolytes, where Li foil was detached after galvanostatic cycling tests at 100 °C. Peaks of Li_2S were observed on the surface of Li_3PS_4 electrolyte after cycling. The Li_3P component was detected on the surface of Li_3PS_4 by P2p XPS measurement, even though the crystalline size of Li_3P may be too small to detect by XRD. Thus, we conclude that Li_3PS_4 glass was reduced to Li_2S and Li_3P by Li metal. The XRD data of $54Li_3PS_4 \cdot 46LiI$ glass still showed a halo pattern after cycling, suggesting that the glassy state was retained.

Fig. 7 shows cross-sectional SEM images of the interfaces of Li/Li_3PS_4 (a, b) and $Li/54Li_3PS_4 \cdot 46LiI$ (c, d) after galvanostatic cycling tests. The secondary electron (SE) images (a, c) and the back-scattered electron (BSE) images (b, d) are displayed. Crack areas with medium-dark contrast were observed between Li metal and Li_3PS_4 glass in the BSE image (b), suggesting the existence of reduced components such as Li_2S and Li_3P. On the other hand, compositional contrasts were not observed at the $Li/54Li_3PS_4 \cdot 46LiI$ interface (d). Furthermore, no cracks and pores were formed at the interface, where good contacts were maintained even after long-term galvanostatic cycling tests for more than 3400 h at 100 °C.

From the results shown in Figs. 6 and 7, the side-reaction with Li metal was suppressed by adding LiI to Li_3PS_4 glass. Crystalline Li_2S with low ionic conductivity of 10^{-8} S cm^{-1} [24] was formed at the

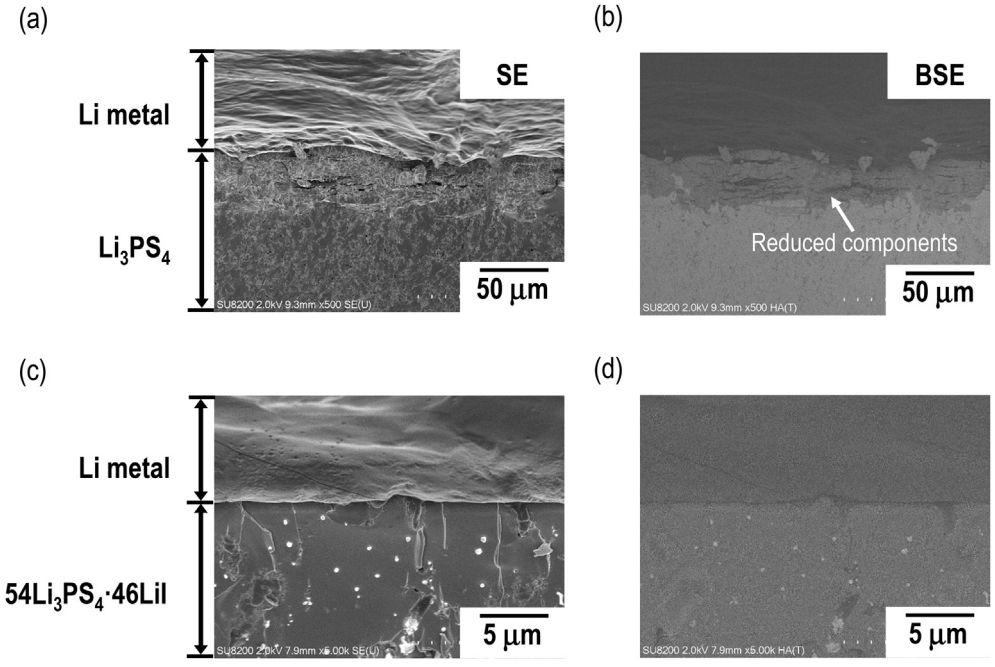

Fig. 7. (a,b) Cross-sectional secondary electron (SE) and back-scattered electron (BSE) images of the Li/Li_3PS_4 interface after galvanostatic cycling tests at 100 °C. (c,d) Cross-sectional SE and BSE images of the $Li/54Li_3PS_4 \cdot 46LiI$ interface after long-term galvanostatic cycling tests as shown in Fig. 3(b).

Li/Li_3PS_4 interface, and this high-resistance layer at the interface may cause the inhomogeneous distribution of current, which induces the formation of Li dendrites. After galvanostatic cycling tests at 100 °C, the formation of reduced species by the side-reaction between Li metal and Li_3PS_4 glass destabilized the Li/Li_3PS_4 interface, as shown in Fig. 7. When Li_3PS_4 glass decomposes into Li_2S and Li_3P, the morphology of the Li/Li_3PS_4 interface changes because of the large volume expansion (~150%) during this decomposition ($Li_3PS_4 + 8Li \rightarrow 4Li_2S + Li_3P$). This may induce the formation of Li dendrites. In contrast, the interface was stabilized by adding LiI to the Li_3PS_4 glass, which effectively prevented the side-reaction with Li metal and helped maintain a close interface during Li dissolution/deposition cycling.

4. Conclusions

All-solid-state Li symmetric cells were fabricated using Li_3PS_4-LiI electrolytes to investigate the Li dissolution/deposition behavior. Li dissolution/deposition performance was improved by adding LiI. A cell using the $54Li_3PS_4 \cdot 46LiI$ glass electrolyte was cycled without short-circuiting at a current density of 1.25 mA cm^{-2} for 3400 h at 100 °C.

XRD and SEM observation indicated the generation of Li_2S at the Li/Li_3PS_4 interface after galvanostatic cycling tests. This generation of Li_2S was suppressed at the $Li/54Li_3PS_4 \cdot 46LiI$ interface, suggesting that side-reaction with Li metal was inhibited by adding LiI to Li_3PS_4 glass. Furthermore, good contacts at the $Li/54Li_3PS_4 \cdot 46LiI$ interface were maintained even after long cycling. Thus, the addition of LiI to Li_3PS_4 glass improved the tolerance to reduction with Li metal and enhanced the Li dissolution/deposition cycling performance.

Acknowledgement

This research was financially supported by the Japan Science and Technology Agency (JST), Advanced Low Carbon Technology Research and Development Program (ALCA), and Specially Promoted Research for Innovative Next Generation Batteries (SPRING) Project.

References

[1] J.M. Tarascon, M. Armand, Nature 414 (2001) 359.
[2] R. Murugan, V. Thangadurai, W. Weppner, Angew. Chem. Int. Ed. 46 (2007) 7778.
[3] J.B. Bates, N.J. Dudney, G.R. Gruzalski, R.A. Zuhr, A. Choudhury, C.F. Luck, J.D. Robertson, J. Power Sources 43 (1993) 103.
[4] M. Tatsumisago, A. Hayashi, Solid State Ionics 225 (2012) 342.
[5] A. Sakuda, A. Hayashi, M. Tatsumisago, Sci. Rep. 3 (2013) 2261.
[6] A. Kato, M. Suyama, C. Hotehama, H. Kowada, A. Sakuda, A. Hayashi, M. Tatsumisago, J. Electrochem. Soc. 165 (2018) 1950.
[7] A. Kato, A. Hayashi, M. Tatsumisago, J. Power Sources 309 (2016) 27.
[8] Y. Zhu, X. He, Y. Mo, ACS Appl. Mater. Interfaces 7 (2015) 23685.
[9] A. Kato, H. Kowada, M. Deguchi, C. Hotehama, A. Hayashi, M. Tatsumisago, Solid State Ionics 322 (2018) 1.
[10] E. Peled, J. Electrochem. Soc. 126 (1979) 2047.
[11] Y.S. Cohen, Y. Cohen, D. Aurbach, J. Phys. Chem. B 104 (2000) 12282.
[12] J. Steiger, D. Kramer, R. Mönig, J. Power Sources 261 (2014) 112.
[13] A. Levasseur, J.C. Brethous, J.M. Réau, P. Hagenmuller, Mater. Res. Bull. 14 (1979) 921.
[14] R. Mercier, J.P. Malugani, B. Fahys, G. Robert, Solid State Ionics 5 (1981) 663.
[15] H. Wada, M. Menetrier, A. Levasseur, P. Hagenmuller, Mater. Res. Bull. 18 (1983) 189.
[16] J.H. Kennedy, S. Sahami, S.W. Shea, Z. Zhang, Solid State Ionics 18–19 (1986) 368.
[17] A. Kato, M. Yamamoto, A. Sakuda, A. Hayashi, M. Tatsumisago, ACS Appl. Energy Mater. 1 (2018) 1002.
[18] E. Rangasamy, Z. Liu, M. Gobet, K. Pilar, G. Sahu, W. Zhou, H. Wu, S. Greenbaum, C. Liang, J. Am. Chem. Soc. 137 (2015) 1384.
[19] F. Yonemoto, A. Nishimura, M. Motoyama, N. Tsuchimine, S. Kobayashi, Y. Iriyama, J. Power Sources 343 (2017) 207.
[20] T. Ohtomo, A. Hayashi, M. Tatsumisago, K. Kawamoto, Electrochemistry 81 (2013) 428.
[21] A. Sharafi, E. Kazyak, A.L. Davis, S. Yu, T. Thompson, D.J. Siegel, N.P. Dasgupta, J. Sakamoto, Chem. Mater. 29 (2017) 7961.
[22] X. Han, Y. Gong, K. Fu, X. He, G.T. Hitz, J. Dai, A. Pearse, B. Liu, H. Wang, G. Rubloff, Y. Mo, V. Thangadurai, E.D. Wachsman, L. Hu, Nat. Mater. 16 (2017) 572.
[23] C.L. Tsai, V. Roddatis, C.V. Chandran, Q. Ma, S. Uhlenbruck, M. Bram, P. Heitjans, O. Guillon, ACS Appl. Mater. Interfaces 8 (2016) 10617.
[24] T. Hakari, A. Hayashi, M. Tatsumisago, Chem. Lett. 44 (2015) 1664.